we make the following spin assignments: 1.27-Mev level spin 2, 2.09-Mev level spin 2, 2.36-Mev level spin 4, 2.49-Mev level spin 2, and 2.75-Mev level spin 4. We further classify the 1.09-Mev, 1.27-Mev, 1.49-Mev, 2.09-Mev gamma rays as quadrupole, the 0.40-Mev transition as a 96% quadrupole, 4% dipole 0° phase, and the 0.80-Mev gamma ray as a 90% quadrupole, 10% dipole 0° phase radiation.

PHYSICAL REVIEW VOLUME 101, NUMBER 2 JANUARY 15, 1956

Nuclear Elastic Scattering of Photons*

E. G. FULLER AND EVANS HAYWARD
National Bureau of Standards, Washington, D. C.
(Received September 16, 1955)

A NaI(Tl) scintillation spectrometer biased to detect only photons in the upper energy tip of a betatron-produced bremsstrahlung spectrum is used to measure the differential nuclear elastic scattering cross section at 120 degrees as a function of photon energy from 4 to 40 Mev. The targets ranged in Z from Na to U. Total cross sections are calculated by assuming a dipole angular distribution. The scattering cross sections tend to exhibit two maxima, one below the particle threshold that corresponds to the scattering by separate levels, and one that follows the giant resonance for photon absorption. Both the maximum cross section and the energy of the giant resonance vary smoothly with A from Na to U and are roughly proportional to $(NZ/A)^2$ and $A^{-1/3}$, respectively. The dipole dispersion relation is used to compare the scattering data with the neutron yield data in the giant resonance region.

I. INTRODUCTION

THE absorption of gamma rays by nuclei has been the subject of numerous investigations. The most recent compilations of experimental data are those given by the Saskatchewan[1] and Pennsylvania[2] groups. Most of this work has involved the measurement of neutron emission cross sections which, when integrated over the "giant resonance," have been compared to the predictions of the dipole sum rule. The elastic scattering process associated with the nuclear absorption of photons presents an alternative way of studying the basic interaction. This paper is an account of an experimental study of the elastic scattering cross section as a function of both energy and atomic number.[3] The results are compared with the neutron yield cross sections.

The scattering of photons in the region of the "giant resonance" was probably first observed by Gaerttner and Yeater[4] and Dressel, Goldhaber, and Hanson.[5] In a more refined experiment[6] Stearns studied the scattering of the Li(p,γ) photons by various nuclei using a NaI(Tl) scintillation counter which detected only the elastically scattered photons. The results indicated that the cross section for the elastic scattering of 17-Mev photons by heavy nuclei is of the order of a few millibarns.

II. EXPERIMENTAL METHOD

The present experiment is an extension of the Stearns experiment. The discrimination level of a large NaI(Tl) scintillation spectrometer is set to detect only the photons in the upper energy tip of the betatron bremsstrahlung spectrum. The spectrometer is first calibrated at a given energy by observing the number of counts, C_1, produced when the spectrometer is placed in the direct beam from the betatron (see Fig. 1). Simultaneously a charge, Q_1, is collected from a transmission ionization chamber in the direct beam. With the detector rotated to the 120° position the number of counts, C_2, produced by scattered photons is recorded while a charge, Q_2, is collected from the ionization chamber. On the assumption that the shape of the bremsstrahlung spectrum is the same for both the high and low intensity beams, the elastic scattering cross section is then given by:

$$\langle\sigma_s\rangle_{\text{Av}}=K(C_2/Q_2)\cdot(Q_1/C_1), \quad (1)$$

where K includes geometrical factors as well as a correction for the absorption of photons in the target. The scattering cross section was determined as a function of energy from 4 to 40 Mev by changing both the peak energy of the betatron and the gain of the amplifier so as to keep the end of the bremsstrahlung spectrum at the same discrimination level. The measured cross

* This research was supported by the U. S. Air Force, through the Office of Scientific Research of the Air Research and Development Command.

[1] Montalbetti, Katz, and Goldemberg, Phys. Rev. **91**, 659 (1953); Summers-Gill, Haslam, and Katz, Can. J. Phys. **31**, 70 (1953); J. Goldemberg and L. Katz, Can. J. Phys. **32**, 49 (1954).

[2] R. Nathans and J. Halpern, Phys. Rev. **93**, 437 (1954); R. Nathans and P. F. Yergin, Phys. Rev. **98**, 1296 (1955).

[3] E. G. Fuller and E. Hayward, Phys. Rev. **94**, 732 (1954); **95**, 1106 (1954); *Proceedings of the 1954 Glasgow Conference* (Pergamon Press, New York, 1955), pp. 155–161. The cross sections given in the present paper differ from those previously published because of an improved estimate of the solid angle.

[4] E. R. Gaerttner and G. L. Yeater, Phys. Rev. **76**, 363 (1949).

[5] Dressel, Goldhaber, and Hanson, Phys. Rev. **77**, 754 (1950).

[6] M. B. Stearns, Phys. Rev. **87**, 706 (1952).

sections are independent of both the shape of the bremsstrahlung spectrum and the response of a monitor.

III. APPARATUS

The physical layout of the experiment is shown in Fig. 1. The repetition rate of the betatron is 180 cycles per second. As operated for this experiment the yield pulse was approximately triangular in shape with a base length of about 10 μsec. The energy to which the electrons in the betatron are accelerated is controlled by a circuit that uses a dc biased peaker transformer to determine when the current in the main coil of the betatron reaches a predetermined value. The energy scale was determined in a separate experiment by observing the (γ,n) thresholds in Be^9 at 1.67 Mev, B^{10} at 8.45 Mev, Cu^{65} at 9.9 Mev, and Cu^{63} at 10.7 Mev. Within the errors of the end-point determinations made during this experiment ($\pm 5\%$), a linear extrapolation of this energy calibration to 40 Mev appears to be valid.

The output from the betatron was monitored by measuring the charge collected from the parallel plate ionization chamber on a polystyrene film condenser. The voltage to which this condenser was charged was measured with a vibrating reed electrometer (Applied Physics Corporation Model 30). To cover the range of beam intensities used, any one of four charge collecting condensers could be switched into the circuit. These ranged in value from about 5.0 to 0.005 microfarads. The ratio of the capacities of these condensers was determined by measuring the time taken for each of them to charge to a given voltage when a radioactive source was placed in a standard position with respect to the chamber. The ionization chamber was checked for saturation effects; none were observed at the highest intensities obtained with the betatron.

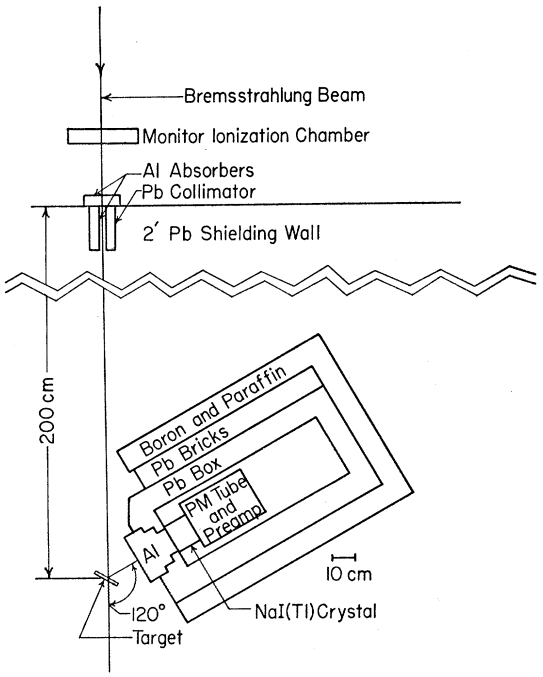

FIG. 1. The experimental arrangement. The detector rotates about a vertical axis through the sample.

The beam was defined by a collimating hole one and one-half inches in diameter through eight inches of lead. This produced a beam four inches in diameter at the target position. The collimating hole was filled with a low-Z material, usually aluminum,[7] to remove preferentially low-energy photons from the bremsstrahlung spectrum.

The detector[8] was a large NaI(Tl) crystal five inches in diameter and four inches long viewed by a Dumont K1198 photomultiplier tube. The crystal, photomultiplier, and cathode follower were all located in a lead container having walls five inches thick surrounded with boxes filled with a mixture of boric acid and paraffin. The counter and its shielding were on a table that could be rotated about a vertical axis through the target position. The crystal viewed the target through a hole five inches in diameter in the shield. This hole contained an aluminum plug four and one-half inches long which filtered out electrons and low-energy photons emitted by the target.

The pulses from the cathode follower were fed by a long cable into the betatron control room where they were amplified and analyzed by a five-channel integral discriminator (Channels A through E) and two differential discriminators (F and G). The amplifier and discriminators were all of conventional design. The outputs of the discriminators were gated so that only those events occurring in a 20-μsec interval around the betatron yield pulse were counted. With this gating the cosmic-ray background was of the order of $\frac{1}{3}$ count per hour in the differential channels. The maximum counting rate in these channels due to photons scattered from the sample was of the order of 20 counts per hour. This rate was limited by the duty cycle of the betatron.

The biases at which the various discriminators were set are indicated in Fig. 2. Also shown in this figure are the pulse-height distributions obtained in the direct beam from the betatron and in the beam scattered by an Al target. At each energy at which measurements were made the detector was first swung into the direct betatron beam and the amplifier gain adjusted until the end point of the pulse-height spectrum produced by the filtered bremsstrahlung beam fell into the differential channel G. The counts registered by F, called the end-point channel, were then used to calculate the elastic scattering cross sections. The other channels, biased above and below F, were useful in monitoring the stability of the equipment and pileup. In all runs the counting rate of discriminator A was used to set the output intensity of the betatron. Pileup in F was experi-

[7] The scattering cross section for Al was measured with a carbon beam filter.

[8] R. S. Foote and H. W. Koch, Rev. Sci. Instr. 25, 746 (1954).

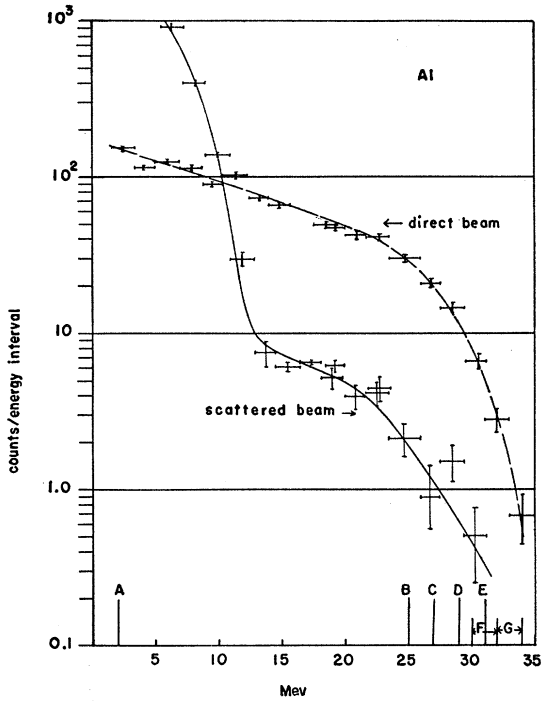

FIG. 2. The pulse-height distributions obtained when the detector is placed in the filtered bremsstrahlung beam and in the beam scattered by an Al target. The peak energy of the betatron was 33 Mev. The levels at which the discriminators fired are indicated by the vertical lines at the bottom. A through E were integral discriminators, and F and G differential discriminators. F is the channel used to determine the elastic scattering cross sections. The sharp rise in the pulse-height spectrum below 12 Mev may probably be attributed to photons resulting from the capture of fast neutrons generated in the target.

mentally found to be negligible if the counting rates in A were kept below 10 per second and 60 per second for runs made in the direct and scattered beams, respectively.

The energy assignment of each measurement was made on the basis of the betatron energy calibration. The firing point of each of the discriminators was first determined with a precision pulser. On the basis of the observed pulse-height distributions in the end-point runs for a particular energy E_0, a pulse-height was assigned to E_0. This pulse height was slightly higher than the firing point of the lower edge of discriminator G. A linear extrapolation was then made to determine the energies to be assigned to the edges of the end-point channel, F. It is felt that these energy assignments are probably good to about 5%.

IV. ANALYSIS OF THE DATA

In order to calculate the cross section, the quantity K in Eq. (1) must be evaluated. Since the targets are of the order of a mean free path thick, a correction for the absorption by the target of photons in both the incident and the scattered beams must be made. The "electronic" absorption processes (i.e., pair production, Compton effect, and photoelectric effect) account for most of this absorption although in some cases it is also necessary to include the effect of the nuclear absorption. In the region of the giant resonance the nuclear absorption cross sections are only a few percent of the "electronic" absorption cross sections and need not be considered.

In the energy region just below the particle thresholds, the observed scattering is presumably due to sharp, well-defined levels. For the lighter nuclei particularly, the maximum nuclear absorption cross section in these levels can reach values of the order of, or possibly greater than, the "electronic" absorption cross section. The maximum value of the dipole absorption cross section in an individual level is $6\pi\lambda\!\!\!^{-2}$. For a 7-Mev photon this gives a cross section of about 100 barns. In any actual case this maximum value will be reduced because of inelastic scattering and the thermal Doppler broadening of the level. Experiments on neutron capture and scattering[9] indicate that the radiation widths, Γ_γ, of nuclear energy levels at excitations of 7 Mev or so are a few tenths of an electron volt. The thermal Doppler width, δ, of a level for 7-Mev photons ranges from 10 electron volts for $A=25$, to 3.6 electron volts at $A=208$. The maximum absorption cross section in the levels is therefore determined chiefly by the Doppler broadening and is given by $\sigma_{\max}\simeq 6\pi\lambda\!\!\!^{-2}\Gamma_\gamma/\delta=1$ barn for nuclei around Mg. This cross section is of the same order as the "electronic" absorption cross section in Mg and therefore contributes appreciably to the absorption of photons in the scattering target.

The effect of absorption in the scattering target on the observed counting rate can be seen in the following way. Consider the scattering from the small element of the target dx as indicated in Fig. 3. The number of counts in the end-point channel from this element is then given by:

$$dC_2=Q_2\frac{C_1}{Q_1}Ndx\Delta\Omega\int_E^{E+\Delta E}dE\frac{\sigma_s}{13.4}f(E)\times e^{-Nx(\sigma_n+2\sigma_e)/\cos\beta}\Big/\int_E^{E+\Delta E}dEf(E). \quad (2)$$

In this expression N is the number of atoms per cm^3 in the target, $\Delta\Omega$ is the average solid angle for detecting a photon scattered by the target, σ_s is the total scattering cross section, σ_n is the nuclear absorption cross section, σ_e is the electronic absorption cross section, and $f(E)$ is the product of the incident photon spectrum and the response of the detector as a function of energy. If the variation of $f(E)$ across ΔE is neglected, Eq. (2) becomes:

$$dC_2=Q_2\frac{C_1}{Q_1}Ndx\frac{\Delta\Omega}{\Delta E}\int_E^{E+\Delta E}dE\frac{\sigma_s}{13.4}e^{-Nx(\sigma_n+2\sigma_e)/\cos\beta}. \quad (3)$$

[9] D. J. Hughes and J. A. Harvey, Nature **173**, 942 (1954).

The number, 13.4, is the ratio of the total cross section to the differential cross section at 120 degrees for an angular distribution of the scattered radiation varying as $(1+\cos^2\theta)$. σ_e is included twice in the exponent of Eq. (2) since both the incident and scattered photon beams are absorbed by electronic processes. As was pointed out above, σ_n is comparable to σ_e only for the scattering by sharp, well-defined levels. In this case the Doppler shift in the photon energy, because of the recoil of the scattering nucleus (10^3 ev for a 7-Mev photon scattered by an Sn nucleus) is so large that it cannot be reabsorbed by the same level in the scattered beam. For this reason the nuclear absorption takes place in the primary beam only.

The solid angle for the detection of a scattered photon depends both on the position of the scattering nucleus within the target and on the depth, t, in the crystal at which the photon is absorbed. It was determined experimentally with a small point source that the mean solid angle averaged over the beam area on the front face of the target was given to a good approximation by the solid angle for detecting a photon scattered by a nucleus at the center of the beam. Neglecting the effect of the finite thickness of the target, the average solid angle for detecting a photon is then

$$\Delta\Omega=\frac{A}{R^2}\int_0^L \frac{e^{-\mu t}dt}{(R+t)^2}\Big/\int_0^L \frac{e^{-\mu t}dt}{R^2}, \qquad (4)$$

where L is the length of the crystal, A is its cross-sectional area, μ is the absorption coefficient of NaI(Tl), and R is the distance from the center of the target to the center of the front face of the crystal. $\Delta\Omega$ is approximately given by $0.82\ A/R^2$ over the energy range from 4 to 40 Mev. The correction to the mean solid angle due to the finite thickness of the targets was calculated to be negligible for the heavy nuclei. For the lighter nuclei this effect decreased the mean solid angle by a maximum of 10% in the case of S. In Table I the properties of the various targets are listed along with the correction, F, applied to the mean solid angle to take account of the finite target thickness.

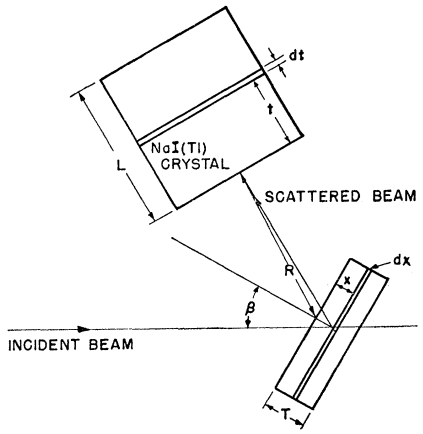

FIG. 3. The geometry.

TABLE I. Target properties.

	T g/cm²	T cm	F[a]
Na	7.1	6.7	0.91
Mg	8.85	5.1	0.93
Al	6.85	2.5	0.96
S	15.5	7.6	0.90
Ca	7.9	5.1	0.92
Mn	10.7	3.8	0.94
Ni	9.45	1.8	1.0
Cu	10.8	1.2	1.0
Sn	6.8	0.93	1.0
I	7.22	1.8	1.0
Au	26.1	1.35	1.0
Pb	14.4	1.27	1.0
Bi	12.3	1.27	1.0
U	26.3	1.42	1.0

[a] F is the factor by which the mean solid angle for detecting a scattered photon is reduced due to the finite thickness of the scattering target (see text).

In order to obtain an expression for an average scattering cross section Eq. (3) may be integrated through the target thickness and rearranged to give

$$\frac{C_2}{Q_2}\frac{Q_1}{C_1}\frac{13.4}{\Delta\Omega\cos\beta}=\frac{1}{\Delta E}\int_E^{E+\Delta E}\frac{\sigma_s}{\sigma_n+2\sigma_e}dE\times[1-e^{-NT(\sigma_n+2\sigma_e)/\cos\beta}]. \qquad (5)$$

Multiplying both sides by $2\sigma_e/[1-e^{-2\sigma_e NT/\cos\beta}]$ yields

$$\frac{C_2}{Q_2}\frac{Q_1}{C_1}\frac{13.4}{\Delta\Omega\cos\beta}\frac{2\sigma_e}{[1-e^{-2\sigma_e NT/\cos\beta}]}\equiv\langle\sigma_s\rangle_{Av}$$
$$=[1-e^{-2\sigma_e NT\cos\beta}]^{-1}\frac{1}{\Delta E}\int_E^{E+\Delta E}\frac{\sigma_s}{1+(\sigma_n/2\sigma_e)}dE\times[1-e^{-NT(\sigma_n+2\sigma_e)/\cos\beta}]. \qquad (6)$$

If σ_n is small compared to $2\sigma_e$ as is true in the region of the giant resonance, $\langle\sigma_s\rangle_{Av}$ is just the scattering cross section averaged over the energy interval ΔE, since σ_e is a slowly varying function of the energy and can be taken outside the integral sign. If, on the other hand, σ_n is not negligible, as is sometimes the case below the particle thresholds, $\langle\sigma_s\rangle_{Av}$ will not be the average scattering cross section, since it does not include an adequate correction for self-absorption in the target. The magnitude of the additional correction for this effect can be obtained from a self-absorption experiment. Preliminary results[10] indicate that in the energy region of the low-energy maximum (see Figs. 4–6) for Mn, Al, Ni, Bi, and Pb the average scattering cross section is approximately 15% higher than the values of $\langle\sigma_s\rangle_{Av}$ obtained from the left side of Eq. (5) and plotted in Figs. 4–6.

[10] E. G. Fuller and E. Hayward, Phys. Rev. 98, 1537 (1955).

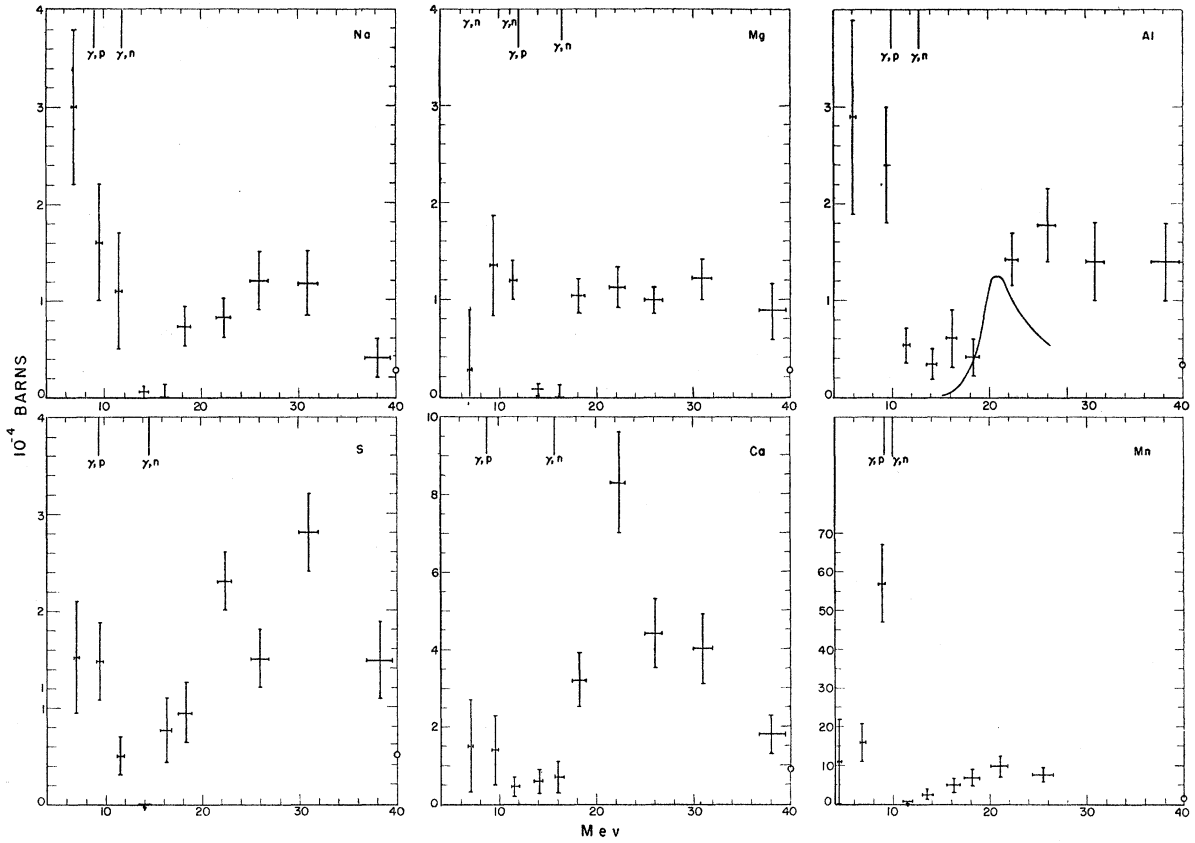

FIG. 4. The elastic scattering cross sections for Na, Mg, Al, S, Ca, and Mn. The indicated spread in energy is the width of the differential discriminator channel, and the standard deviations are based only on the number of counts. The vertical lines at the top represent the particle thresholds for the most important isotopes. The open circles at the extreme right indicate the magnitude of the Thomson cross section for Z free protons scattering coherently. The solid curve superimposed on the Al data is the scattering cross section calculated from the dispersion relation by substituting for $\sigma_a(E)$ in Eq. (6) the sum of the neutron and proton yield[1,15] cross sections.

V. RESULTS AND DISCUSSION

The experimental results are plotted in Figs. 4–5. The indicated spread in energy is the width of the end-point channel. The mean energy corresponding to each point is not necessarily at the center of the channel because of the variation of the scattering cross section, the response of the detector, and the incident photon spectrum over ΔE. The indicated uncertainties in the cross sections are the standard deviations based only on the number of counts. Systematic errors in the absolute cross sections may be as large as 15%. These would not affect the relative cross sections at different energies or for different elements. The largest uncertainty is probably in the estimate of the solid angle.

The measured elastic scattering cross sections are, of course, the result of the interference between the coherent processes, Rayleigh, Delbruck, nuclear resonant, and Thomson scattering. Since the present experiment was done at a backward angle, Rayleigh and Delbruck scattering, associated with electronic absorption processes, are negligible and only the scattering by the nuclear charge distribution need be considered. In the low-energy limit this is just the Thomson scattering cross section for a rigid charge of mass A and charge Z, $(8\pi/3)(Z^2e^2/AMc^2)^2$. In the high-energy limit the cross section is that for Z free protons scattering coherently, i.e., the scattering by a rigid charge of mass Z and charge Z, $(8\pi/3)(Ze^2/Mc^2)^2$. At intermediate energies the nuclear resonant scattering results from the elastic deformation of the nuclear charge distribution. The magnitude of the nuclear Thomson scattering cross section is usually small compared to the experimentally measured scattering but on the high side of the giant resonance, the scattering cross section may be approaching the Thomson cross section for Z free protons, indicated by the open circles on the right side of Figs. 4–6.

The measured elastic scattering cross sections all rise smoothly to a maximum above the particle emission thresholds of the scattering nuclei. For the lighter elements ($A<50$) these maxima bear little resemblance to the giant resonance curves obtained from the photoneutron experiments. For the heavier nuclei ($A>50$), however, the scattering curves follow the trend of the

giant resonance obtained from the neutron emission experiments. The magnitude of the scattering cross section at the peak is a smooth function of A varying from 0.12 mb for Na to 15 mb for Pb. Many of the elements studied also have a secondary maximum in the cross section below the particle threshold where the scattering is comparable to that in the giant resonance region. The ratio, R, of the peak cross section in this low-energy maximum to that at the peak of the giant resonance is given in Table II. The wide variations in this ratio, in contrast to the smooth trend of the peak scattering cross section in the giant resonance, indicate that the scattering below the particle thresholds reflects individual nuclear properties rather than the gross properties of nuclear matter that describe the giant resonance.[11] These individual properties show up most markedly in the self-absorption experiment[10] where the analysis of the data yields information about mean radiation widths and level densities.

The qualitative features of the scattering curves can be understood as follows: At excitations below the particle thresholds the nucleus can lose its energy only by photon emission, either by a transition directly to the ground state or by transitions to intermediate states. The size of the low-energy maximum in the scattering cross section then depends in part on the number of alternative modes of decay available for the excited nucleus and therefore on the details of the level structure in the particular scattering nucleus. As the energy of excitation is increased above the particle threshold the scattering cross section drops sharply because of competition with particle emission. This result is in agreement with the qualitative prediction of Bethe and Ashkin.[12] At still higher energies the average ratio of photon emission to particle emission becomes constant and the cross section rises again to follow the trend of the oscillator strength distribution in the giant resonance.

The shape of the elastic scattering cross section in the giant resonance region may be compared with the shape of the cross section for neutron production obtained from other betatron experiments. For the heavier elements, $A>50$, the widths and positions of the peaks of the cross sections displayed in Figs. 4–6 are very similar to the corresponding quantities obtained from the neutron yield cross sections. For the lighter nuclei, $A<50$, however, the scattering cross section curves are considerably broader and peak at much higher energies than would be suggested by the neutron yield data.[1,2,13] For example, the neutron yields cross section for aluminum peaks near 20 Mev, and has a width of about 2 Mev; whereas the elastic scattering cross section has a broad maximum located near 28 Mev. The energy that corresponds to the center of the oscillator strength

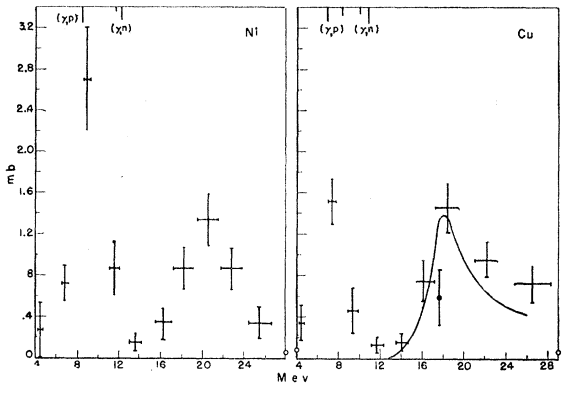

FIG. 5. The elastic scattering cross sections for Ni and Cu. The point at 17.6 Mev is that of Stearns.[6] The solid curve superimposed on the Cu data is the scattering cross section calculated from the dispersion relation by substituting for $\sigma_a(E)$ in Eq. (7) the (γ,n) cross section[1] multiplied by the ratio of the total particle yield to the neutron yield.[16] The open circles on the vertical axes indicate the magnitude of the Thomson cross section for Z free protons scattering coherently.

TABLE II. Comparison of cross sections. R is the ratio of the peak cross section below the particle thresholds to that at the peak of the giant resonance. $\sigma(\gamma,n)$ and σ_s are the neutron yield cross section and the scattering cross section at the peak of the giant resonance, respectively. σ_T is $\sigma(\gamma,n)$ multiplied by the ratio of the total particle yield to the neutron yield. $6\pi\lambda\!\!\!^{-2}$ is evaluated at the energy corresponding to the peak of the giant resonance.

	1 R	2 $\sigma^2(\gamma,n)/\sigma_s$ barns	3 σ_T^2/σ_s barns	4 $6\pi\lambda\!\!\!^{-2}$ barns	Reference
Na	2.5				
Mg	1.0				
Al	1.6				
S	0.5				
Ca	0.2				
Mn	5.7	13.7		21	1
		14			2
Ni	2.8	2.5	10	22	1, 15
Cu	1.0	9.8	19	23	1, 16
Sn	3.8				
I	0.27	30		32	1
		8.5			2
Au	0.3	46.5		36	1
		19.3			2
Pb	1.2	53		44	1
		40			2
Bi	1.9	74		44	1
		35			2
U	0.3	40		40	2

[11] Since the capture of slow neutrons in the detector will produce photons of about 7 Mev, some consideration has been given to the possibility that some of the counts observed at this energy might result from neutron capture gamma rays. The counting rates with the sample removed from the x-ray beam were negligible so that background neutrons produced in the betatron and its shielding contributed little. With the scattering target in the beam the observed relative counting rates were consistent neither with the slow or fission neutron capture cross sections, nor with the fast neutron scattering cross sections for the target nuclei. Neutrons accompanying the x-ray beam captured in the target, or scattered into the detector by the target, probably then contribute a negligible amount to the observed counting rate. In the case of Sn and Pb the observed low-energy maximum in the scattering cross section is at an energy slightly above the (γ,n) threshold for about 20% of target nuclei. Extremely rough estimates indicate that no more than 15% of the counting rate from Sn and Pb resulted from photoneutrons produced in the scattering target.

[12] H. Bethe and J. Ashkin, *Experimental Nuclear Physics*, edited by E. Segrè (John Wiley and Sons, Inc., New York, 1953), Vol. 1, p. 347.

[13] Ferguson, Halpern, Nathans, and Yergin, Phys. Rev. **95**, 776 (1954).

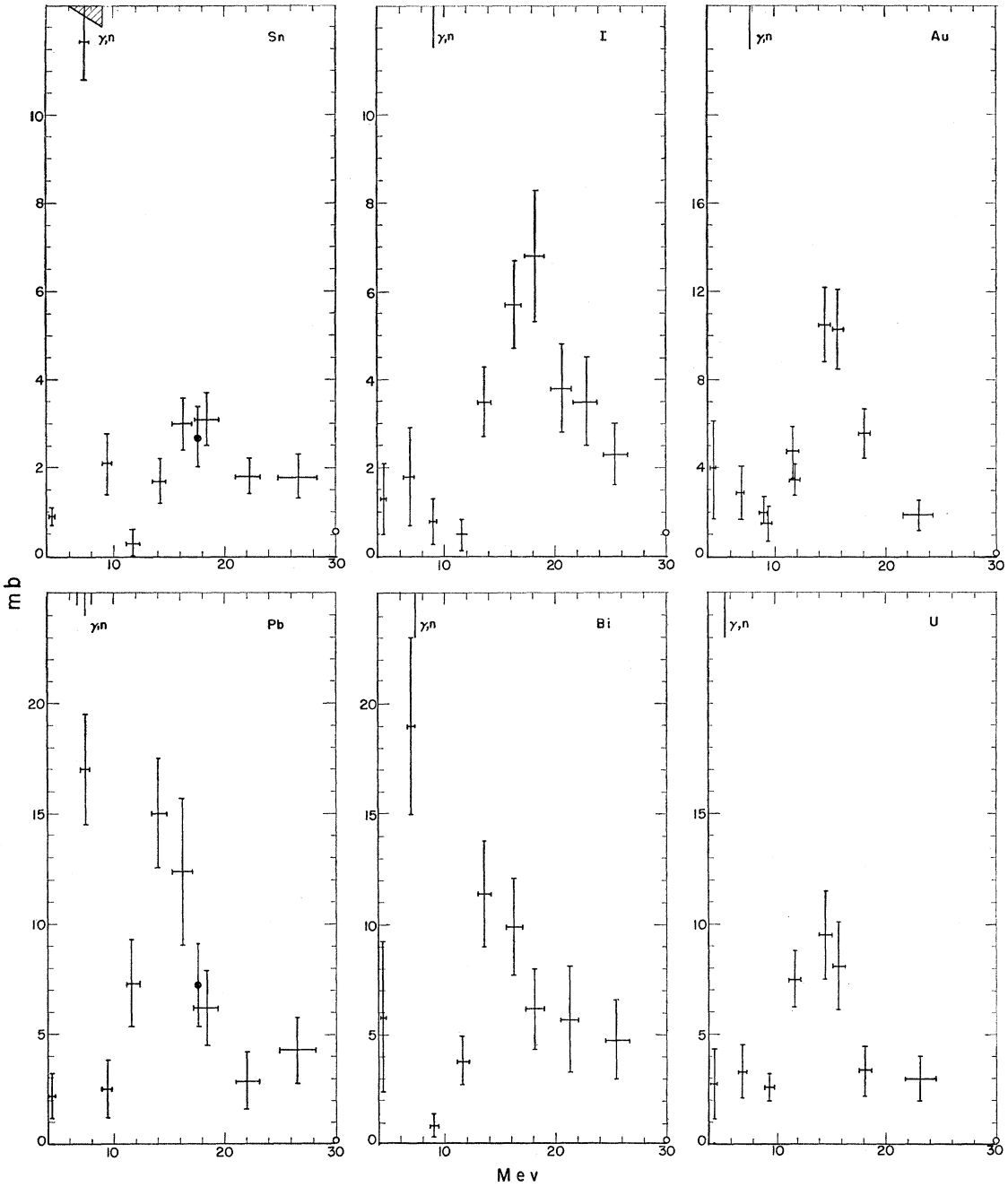

FIG. 6. The elastic scattering cross sections for Sn, I, Au, Pb, Bi, and U. The points at 17.6 Mev are those of Stearns.[6]

distribution as determined from the scattering cross sections is plotted as a function of A in Fig. 7. The line drawn through the points corresponds to the dependence,

$$E_m = 82A^{-1/3}, \quad (7)$$

which is consistent with what is to be expected on the basis of simple hydrodynamical considerations.[14]

A detailed comparison of the scattering data and the neutron yield data can best be made in terms of the dispersion relation that gives the dependence of the elastic scattering cross section in the forward direction on the total photon absorption cross section.[15] If the transitions involved in the scattering and absorption are dipole, this leads to the following relationship

[14] M. Goldhaber and E. Teller, Phys. Rev. **74**, 1046 (1948); H. Steinwedel and J. H. D. Jensen, Z. Naturforsch. **5a**, 413 (1950); Ferentz, Gell-Mann, and Pines, Phys. Rev. **92**, 836 (1953).

[15] Gell-Mann, Goldberger, and Thirring, Phys. Rev. **95**, 1612 (1954).

between the elastic scattering cross section, $\sigma_s(E)$, and the total absorption cross section, $\sigma_a(E)$:

$$\sigma_s(E)=\frac{1}{6\pi\lambda^2}\left[\sigma_a^2(E)+\left(\frac{2E}{\pi}P\int\frac{\sigma_a(E')dE'}{E'^2-E^2}\right)^2\right]$$
$$+\frac{8\pi}{3}D^2+\frac{8}{3\pi}\frac{1}{\hbar c}DE^2P\int\frac{\sigma_a(E')dE'}{E'^2-E^2}, \quad (8)$$

where D is the Thomson scattering amplitude. The measured scattering cross sections are really averages of the right side of Eq. (8) over an energy band 1 to 2 Mev wide. As long as σ_a is a smooth function of the energy, as it is in the giant resonance region, all of the cross sections appearing in the above expression may be replaced by their average values, since $\langle\sigma_a^2\rangle_{Av}\simeq\langle\sigma_a\rangle_{Av}^2$. The average scattering cross section can then be calculated from the average absorption cross section. If, on the other hand, the absorption cross section varies rapidly in ΔE, the average scattering cross section will be large compared to that obtained by substituting the average absorption cross section in the dispersion relation.

In order to determine how well the elastic scattering cross section may be predicted from the available photon absorption cross sections, $\sigma_s(E)$ has been calculated by substituting the measured values of $\sigma_a(E)$ for Al and Cu in Eq. (8). The total absorption cross section for Al was taken to be the sum of the (γ,n) and (γ,p) cross sections.[1,16] The total absorption cross section for Cu was taken as the product of the (γ,n) cross section and the ratio of the integrated total particle yield to the integrated neutron yield given by Byerly and Stephens.[17] The results of these calculations are given by the solid curves in Figs. 4 and 5. It may be seen that $\sigma_s(E)$ for Cu can be predicted satisfactorily from the published photon absorption cross sections. The results for Al indicate that the Al nucleus must absorb photons at considerably higher energies than is implied by the available neutron and proton yield data.

If the absorption cross section, σ_a, has a resonance shape then there is some energy near its peak for which the terms involving the integrals in Eq. (8) vanish and

$$\frac{\sigma_a^2}{\sigma_s-(8\pi/3)D^2}=6\pi\lambda^2. \quad (9)$$

This expression may be used to compare the elastic scattering data with the neutron yield data at the peak of the giant resonance in order to obtain an indication of how well the total absorption cross section is represented by the (γ,n) cross section. In making this comparison, the nuclear Thomson scattering cross section $(8\pi/3)D^2$, is neglected since it is small compared with the uncertainties in the measured scattering cross sections. The ratio, $\sigma^2(\gamma,n)/\sigma_s$ at the peak of the giant resonance is given in column 2 of Table II for the heavier elements ($A>50$). This ratio is not given for $A<50$ because of the large differences in the shapes of the (γ,n) and scattering cross sections and the resultant ambiguities in the meaning of the ratio. Within the errors in the experimental determinations of $\sigma(\gamma,n)$ and σ_s, Eq. 9 is satisfied for all of the heavier nuclei. As is indicated in column 3, better agreement is obtained for Cu and Ni if the ratios given in column 3 are multiplied by the square of the ratio of the neutron plus proton yield cross section to the neutron yield cross section.[16,17]

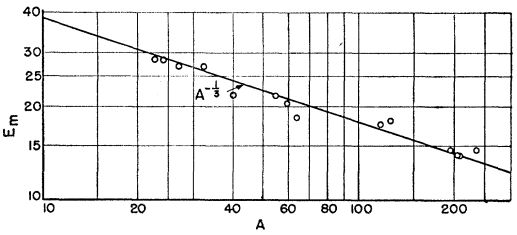

FIG. 7. The dependence of E_m on the atomic mass number A. E_m is the energy of the center of the giant resonance of the scattering curves given in Figs. 4–6. The line drawn through the points corresponds to the dependence $E_m=82A^{-1/3}$.

Equation (7) may be rearranged and integrated to give

$$6\pi c^2\hbar^2\int\frac{\sigma_s(E)}{E^2}dE=\int\sigma_a^2(E)dE$$
$$+\int dE\left|\frac{2E}{\pi}P\int\frac{\sigma_a(E')dE'}{E'^2-E^2}\right|^2. \quad (10)$$

In this expression the integral of the Thomson scattering cross section, $(8\pi/3)D^2$, has been neglected because this cross section is small compared to any of the measured scattering cross sections. The last term in Eq. (8) is also omitted since contributions from either side of the giant resonance tend to cancel in the integration. In the case of Al and Cu the integral of this term was less than 10% of the two remaining terms in Eq. (8).

Both sides of Eq. (10) have been crudely evaluated using the scattering cross sections measured in the present experiment and the published neutron yield cross sections[1,2] for the same elements. The integrations were done only over the giant resonances, i.e., from the (γ,n) threshold to 25 Mev for $A>50$ and to 40 Mev for $A<50$. The contribution from the sometimes large scattering cross section below the threshold was omitted since it results from the absorption by lines having widths small compared to their spacing and for which the substitution of $\langle\sigma_a\rangle_{Av}^2$ for $\langle\sigma_a^2\rangle_{Av}$ is not valid.

The results of these integrations divided by $(NZ/A)^2$ are compared in Fig. 8. Since $\int\sigma_a dE=0.06NZ/A\times(1+0.8x)$, the integrals of Eq. (10) should be roughly proportional to $(NZ/A)^2$ and the points of Fig. 8 should

[16] J. Halpern and A. K. Mann, Phys. Rev. 83, 370 (1951).
[17] P. Byerly and W. E. Stephens, Phys. Rev. 83, 54 (1951).

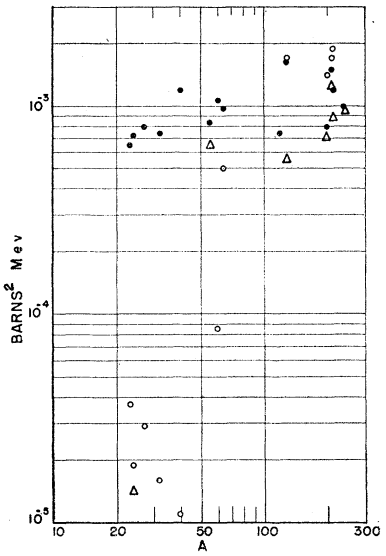

FIG. 8. A plot of the integrals of Eq. (10) as a function of A. The dots are the left side of Eq. (10) divided by $(NZ/A)^2$ obtained from the data of the present experiment. The open circles and triangles are the right side of Eq. (10) divided by $(NZ/A)^2$ obtained from the neutron yield data of references 1 and 2, respectively.

lie on a horizontal line the height of which is determined by the sum rule.[18] The points obtained from the scattering data are all consistent with those obtained from the neutron yield data for the heavy elements for which the integrated neutron yield cross sections are known to exhaust the dipole sum.

The values of the scattering integrals for the low-Z nuclei extrapolate smoothly from the values obtained for the heavier nuclei. This is in contrast to the results obtained for the integrals of the neutron yield cross sections where the values fall off markedly below $A=50$. The high values of the scattering integrals for Na, Mg, Al, S, and Ni can, of course, be explained by assuming that all of the photon absorption for these nuclei is due to sharp, well-defined levels. It would be a remarkable coincidence, however, if the strengths and distributions of the levels in these five nuclei would have just the right values for the scattering integrals to fall on a smooth extrapolation of the values obtained for the heavier nuclei. A more reasonable explanation would be that the absorption cross section for these nuclei is made up principally of a smooth slowly varying function of the energy. These data then indicate that the (γ,n) cross section represents only a fraction of the total absorption cross section.

[18] J. S. Levinger and H. A. Bethe, Phys. Rev. 78, 115 (1950).

The integrals evaluated from the neutron yield data can be corrected to include proton emission by multiplying them by the square of the ratio of the neutron plus proton yield to the neutron yield.[1,2,16,19] This raises the points for Mg to 2.7×10^{-4} and 2.0×10^{-4} barns^2 Mev, and the points for Al, S, Ca, and Ni to 1.2, 4.9, 6.6, and 3.4×10^{-4} barns^2 Mev, respectively. After correction for the proton yields the absorption integrals for Mg, Al, and Ni are still below the scattering integrals by a factor of approximately three. The integrals for S and Ca are in agreement with the scattering integrals. It should be pointed out that for Al and Ni the corrections were made using the actual (γ,n) and (γ,p) cross sections as a function of energy.[1,16] For Mg, S, and Ca the corrections involve the use of data obtained from the ratio of the proton yeilds produced by a 28-Mev bremsstrahlung spectrum to that produced by a 23.5-Mev bremsstrahlung spectrum.[19] The agreement of the integrals (S and Ca) calculated from the scattering data and the absorption data corrected for proton emission may be fortuitous in view of the fact that the absorption cross sections used in calculating the integrals both peaked below 22 Mev while the scattering data indicate that there is considerable absorption at energies above 24 Mev.

In conclusion, the data of this experiment indicate that both the scattering integral and the energy corresponding to the center of the oscillator strength distribution vary rather smoothly from Na to U. This is in contrast with the data obtained from the neutron yield experiments where both the integrated cross sections and the energies of the maxima in the yield curves start to fall below the values predicted by the sum rule and simple hydrodynamical considerations for nuclei less than about $A=50$. The scattering data indicate that the giant resonance for the light nuclei is both considerably broader and centered at a higher energy than the presently available data on the (γ,p) and (γ,n) reactions would imply. In this connection it should be pointed out that no extensive measurements of the particle yield cross sections have been made at energies greater than 24 Mev.

ACKNOWLEDGMENTS

The authors thank Dr. U. Fano and Dr. H. W. Koch for their continued interest and support, and N. Svantesson for his collaboration in some of the latter phases of the work. Special thanks go to Dr. M. Danos for many very fruitful discussions.

[19] S. A. E. Johansson, Phys. Rev. 97, 1186 (1955).